# More On "What Would Be Inside of M87* to Explain the Event Horizon Telescope (EHT) Results ?"

Stefan Mehedinteanu

**More On "What Would Be Inside of M87* to Explain the Event Horizon Telescope (EHT) Results ?"**

Stefan Mehedinteanu[1]

Stefan Mehedinteanu[1]
CITON — Center of Technology and Engineering for Nuclear Projects
Atomistilor no. 409, Bucharest-Magurele, Romania
[1] (retired), E-Mail: mehedintz@yahoo.com

**Abstract**
Since the Hawking radiation is negligible
($T = \eta\kappa/k2\pi \cong 10^{-17}\,K$, $\kappa = c^3/4GM \cong 10^{-5}[s]^{-1} - surface\_gravity$, $M = 2\times 10^9 M_{SuN}$),
another solutions are searched to explain the strong emission of M87*, one of them being to use the older models about the extraction of the Kerr BH internal energy as due of the accretion disk electro-magnetic flux.
Here, as in the previously author's work, see ref. [39]: **What Would Be Inside of M87* to Explain the ~~VHT~~ EHT Results** ?", we explain this emission as follow with some new supplements which strengths the as used models.
Why I obtained such results, the miracle is that I used more intuitively a lot of new ingredients developed by a lot of authors (many cited here) as : Anti de Sitter/Conformal Field Theory (Ads/CFT) correspondence and Kerr/CFT, respectively. The space-time deformation being analyzed in terms of he holographic entanglement via bit threads flux lines (possible open strings with quarks ends on CFT-boundary) it could be viewed as the common cause for almost of cosmic Universe epochs, as Electroweak Phase Transition (EWPT), CMBR and Confinement, others events like Black holes (BHs) merging and the lensing effects.
But what are the physical basis of entanglement bulk-boundary, or of this "spooky action at distance", which exists, since its consequence-the light bending around cosmic bodies is a real fact!
Thus, all the known parameters of **M87*** Event Horizon Telescope (EHT) Results are explained in terms of these new models.

## 1. State of art

From " First M87 Event Horizon Telescope (EHT) Results" [1], we can extract the followings:
"The horizon-scale emission of M87 at 1.3 mm exhibits a robust crescent-like structure. The global very long baseline interferometry (VLBI) at an observing wavelength of 1.3mm (230 GHz) with Earth-diameter-scale baselines is required to resolve the shadows of the core of M87.
The crescent morphology, rapid drop to a deep interior flux depression, and broad consistency among days, methods, and the stellar dynamics measurement all point to the emission structure from M87 being due to strong gravitational lensing around a central black hole.

VLBI observations at 1.3mm have revealed a diameter of the emission region of $\cong 40\mu as \cong 1.2\times 10^{12}[m]$, which is comparable to the expected horizon-scale structure.
Finally, the radio core in M87 is quite typical for powerful radio jets in general.
This measurement from lensed emission near the event horizon is consistent with the presence of a central Kerr black hole, as predicted by the general theory of relativity.
In [1] they present in Section 3 a pedagogical description showing how within compact ring models the emission diameter and central flux depression (shadow) can be inferred directly from salient features of the visibility data" .
In some refs cited in [1], is shown that "in many Active galactic nuclei (AGNs), collimated relativistic plasma jets (Bridle &Perley 1984; Zensus 1997) launched by the central black hole contribute to the observed emission. These jets may be powered either by magnetic fields threading the event horizon, extracting the rotational energy from the black hole (Blandford & Znajek 1977), or from the accretion flow (Blandford &Payne 1982). The near-horizon emission from low-luminosity active galactic nuclei (LLAGNs); Ho 1999) is produced by synchrotron radiation that peaks from the radio through the far infrared. This emission may be produced either in the accretion flow (Narayan et al. 1995), the jet (Falcke et al. 1993), or both (Yuan et al. 2002) ".
In [1] the appearance of M87* has been modeled successfully using general-relativistic Magnetohydrodynamics (GRMHD) simulations, which describe a turbulent, hot, magnetized disk orbiting a Kerr black hole. They naturally produce a powerful jet and can explain the broadband spectral energy distribution observed in LLAGNs. At a wavelength of 1.3 mm, and as observed here, the simulations also predict a shadow and an asymmetric emission ring.
In my opinion, from these models do not result what is inside the BH, and by what mechanism the inside gravitational and matter gives the spacetime deformation (BH extension) and the horizon emission.
In the following we will come with new models in the spirit of more common physical raisons used in cosmology, as a combination of, the inflation, the electroweak phase transition (EWPT) Universe epoch (~100GeV~0.1m), when the BH is viewed as spacetime region, the origin and the content of black holes (BHs) as mainly strings ended in quarks, FLRW, the entanglement hologram, all being experienced by the author himself in recent works, in order to explain the Earth lensing, the CMBR appearance and frequency, LIGO strain, etc. [15÷18], and the companion references mentioned therein, and repeated here.
Thus, in [ 24], from a universal entropy bound found in cited ref. [1], is obtained a background independent formulation of the holographic principle, cited refs [10,11]. This led us to a construction of hypersurfaces (screens) on which all information contained in a space-time can be stored. The screens are embedded, or lie on the boundary of the space-time, and contain no more than one bit of information per Planck area. In this sense, the world is a hologram.
In [24], is provided a background-independent formulation of the holographic principle. It permits the construction of embedded hypersurfaces (screens) on which the entire bulk information can be stored at a density of no more than one bit per Planck area. Screens are constructed explicitly for AdS, Minkowski, and de Sitter spaces with and without black holes, and for cosmological solutions. The properties of screens provide clues about the character of a manifestly holographic theory. Therefore, we can use the holographic

principle (which refers to $N_{dof}$ ) to project all information in the space-time onto screen-hypersurfaces.
The construction was applied to a number of examples. For Anti-de Sitter space it yields the timelike boundary at spatial infinity as a preferred screen.
From [25], the generalized covariant entropy bound is the conjecture that for any null $k^a \equiv (d/d\lambda)^a$ hypersurface which is generated by geodesics with non-positive expansion starting from a spacelike 2-surface B and ending in a spacelike 2-surface B′, the matter entropy on that hypersurface will not exceed one quarter of the difference in areas, in Planck units, of the two spacelike 2-surfaces. It is shown that this bound can be derived from the following phenomenological assumptions: (i) matter entropy can be described in terms of an entropy current $s_a$; (ii) the gradient of the entropy current is bounded by the energy density, in the sense that $\left|k^a k^b \nabla_a s_b\right| \le 2\pi T_{ab} k^a k^b / \eta$ for any null vector $k_a$, where $T_{ab}$ is the stress energy tensor; and (iii) the entropy current $s_a$ vanishes on the initial 2-surface B.

The "irreducible" mass of BH [28], which is proportional to the area of horizon, is interpretable as the entropy when Hawking's quantum emission is negligible. The extraction of the "reducible" mass of a Kerr hole in presence of strong magnetic field supported by external currents (charged particles $e^- - e^+$ created ) flowing in the equatorial disk, which is supposed to be Keplerian, it could be possible with pairs generation.

In [36], according to the AdS/CFT prescription, the expectation value of the boundary stress-energy tensor is determined by functionally differentiating the on-shell gravitational action with respect to the boundary metric.
Most of the discussions in the literature on the AdS/CFT correspondence are concerned with obtaining conformal field theory correlation functions using supergravity. In this paper they started investigating the converse question: how can one obtain information about the bulk theory from CFT correlation functions? How does one decode the hologram?
In two dimensions they obtain

$$\left\langle T_{ij} \right\rangle = \frac{l}{16\pi G_N} t_{ij}$$

As promised, $t_{ij}$ is directly related to the boundary stress-energy tensor.

Taking the trace we obtain

$$T_i^{\ i} = -\frac{c}{24\pi} R$$

Where the central charge $c = 3l/2G_N$ which is the correct conformal anomaly [10] cited.
In this section we wish to examine how field theory describing matter on this spacetime is encoded in the CFT. In this section we wish to examine how field theory describing matter on this spacetime is encoded in the CFT.

According to cited [11] the quasi-local stress-energy tensor is not conserved in the presence of matter but it satisfies:

$\nabla^j \langle T_{ij} \rangle = -\tau_{i\rho}$

where $\tau_{i\rho}$ expresses the flow of matter energy-momentum through the boundary.

**2. The Gravito-Electric Einstein Tensor in Core of BH**

In the case of a homogeneous potential directed along the z-axis [10] eq. (2.2), the Einstein stress-energy tensor is:

$$T^{00} = T^{11} = T^{22} = -T^{33} = \rho = \frac{\varepsilon_0 c^2 B^2}{8\pi};\ T^{0i} = 0, \qquad (1)$$

where $\rho_B[J/m^3]$-the magnetic energy density.

$$\varepsilon = \frac{V_{vol}\varepsilon_0 c^2 B^2}{8\pi} = \rho V_{vol} = V[J], \qquad (2)$$

$V_{vol} = 2\pi\lambda_C \lambda_c (4\lambda_C) \cong 8\pi\lambda_C^3$, at Compton length equally with the penetration length $\lambda_C = \lambda$, that results

$$E^2 = \frac{(V)}{\varepsilon_0 (\lambda_C^{e*})^3} \qquad (3)$$

With $V = \varepsilon_{gluons}$ as above is obtained $B = E_{q\bar{q}}/c$.

$$\varepsilon = \frac{V_{vol}\varepsilon_0 c^2 B^2}{8\pi} = \rho_B V_{vol} = V = m_A = [J], \qquad (4)$$

$V_{vol} = 2\pi\lambda_C \lambda_c (4\lambda_C) \cong 8\pi\lambda_C^3$, at Compton length $\lambda_C = \eta/mc$

$$E^2 = \frac{(V)}{\varepsilon_0 (\lambda_C^{e*})^3} \ , \text{ also } E = Bc = \frac{\eta c}{e\lambda_C^2} \qquad (5)$$

Here, the Hubble constant is defined as

$$H^2 = \frac{1}{R_{Earth}^2} = \frac{8\pi G V^4}{3(\eta c)^3 c^4} \to \frac{8\pi G V^4}{3\lambda_C^3 (mc^2)^3 c^4} \to \frac{8\pi G}{3}\frac{V}{\lambda_C^3 c^4}[m^{-2}] \qquad (6)$$

Or based on bit-threads [15÷18] as

$$\frac{c^3 \cdot \rho \cdot l_P^2}{3\eta}\frac{1}{c^2} = H^2[m^{-2}] \qquad (7)$$

$\eta = 10^{-34}[Js]$

$$\rho\big|_{bulk} = n_{bit\_threads}\rho_{bubble} = n\rho = n\frac{T_j}{c^2\lambda_C^3}$$

For example, $\rho = \dfrac{M_U}{n_{bit\_threads} \cdot \lambda_C^3 \cdot a_{end}^2}$; (8)

$n = n_{bit\_threads} = \dfrac{M_U c^2}{m_A \cdot a_{end}}$ ; the Compton length $\lambda_C = \eta/m_A c$

To note following [38] that for the present field content the variation of the total Hamiltonian splits into a (non-vanishing) term associated to the background metric and one associated to the matter fields

$$\delta H_\zeta = \delta H^g_\zeta + \delta H^m_\zeta$$

So, in the following we will consider the both contributions.

We would now like to suggest that a thread that emanates from a region *A* on the boundary (and does not return to it) should be thought of as a channel that can carry one independent bit of information about the microstate of *A*.
The Ryu-Takayanagi entanglement entropy formula [1,29], [37] is by now a firmly established entry in the holographic dictionary. This formula, which applies when the bulk is static and governed by classical Einstein gravity,1 gives the EE of an arbitrary spatial region *A* in terms of the area of *m(A)*, the minimal bulk surface homologous to *A* (Fig. 1):

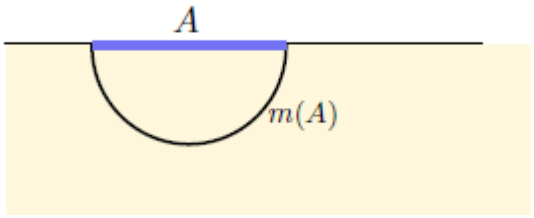


$$S(A) = \frac{1}{4\pi G}\, area(m(A)) \qquad (1.1)$$

**Fig. 1** according to the Ryu-Takayanagi formula, (1.1) from [3], the entanglement entropy *S(A)* of a given boundary spatial region is given by the area of a corresponding bulk minimal surface *m(A)*

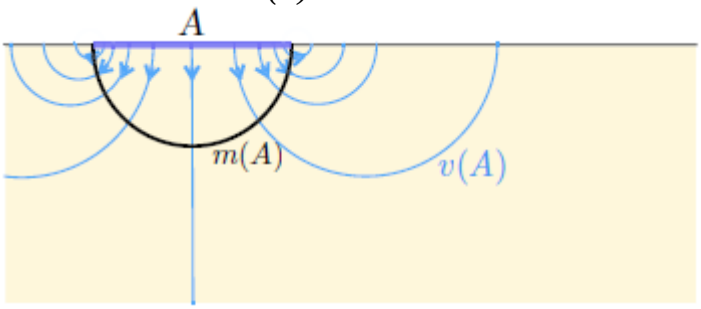


**Fig. 7.** According to Eq. (2.8) from [3] , the entanglement entropy of the region *A* is given by the maximum flux through *A* of any flow. A maximizing flow *v(A)* is illustrated by its flow lines in *blue*. This flux will equal the area of the RT minimal surface *m(A)* (divided by 4*G*N).

$$S(A) = \max_v \int_A v \qquad (2.8)$$

Very recently, Freedman and Headrick suggested that the computation of entanglement entropy can be reinterpreted in terms of a specific convex optimization problem [3]. More

specifically, they showed that the problem can be cast in terms of finding a bulk vector field $v$ with maximum flux through the corresponding boundary region, divergenceless $\nabla.v = 0$, and with an upper bound set by the Planck scale $|v| \leq 1/4G_N$ .

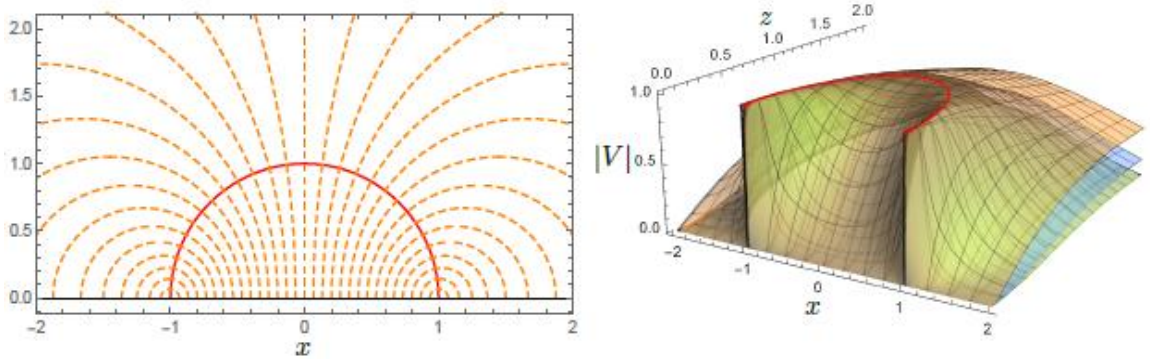


Figure 2. Vector lines and magnitude $|V|$ for a sphere in d = 1 (orange), d = 2 (blue) and d = 3 (green) spatial dimensions, respectively. The vector field $V$ exhibits spherical symmetry so, for simplicity, we have plotted only one of the spatial axis in all case. The solid red line corresponds to the minimal surface, $m(A)$. This curve also signals the location where the magnitude of the vector field attains its maximal value, $|V| = 1$.

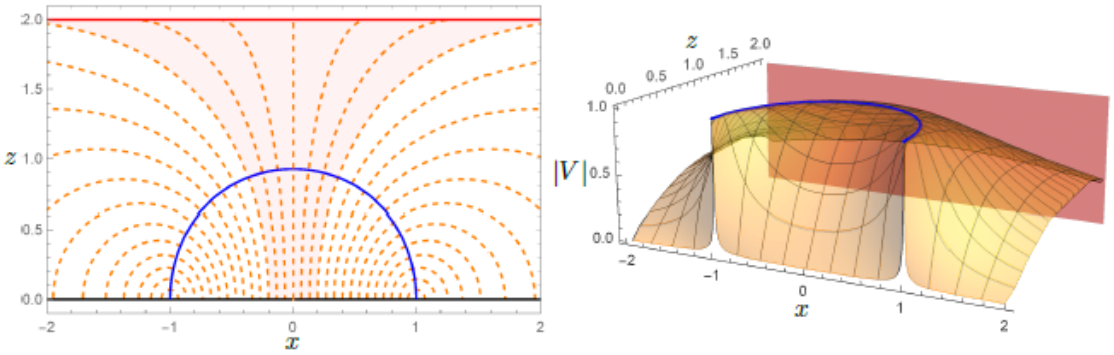


Figure 4 from [40]. Typical integral curves and magnitude $|v|$ in a BTZ black hole geometry. The solid lines in blue correspond to the minimal surface, m(A), and precisely at this location the magnitude of the vector field attains its maximal value, $|v| = 1$. The vector lines in the shaded region correspond to threads that end at the horizon, while the the ones in the white area correspond to threads that go back to the boundary.

For non-vacuum solutions, Einstein's equations with an appropriate stress-tensor, the Ricci on a constant-t slice for negative cosmological constant $\Lambda < 0$, we have that R < 0 if and only if the local energy density is bounded from above:

$$\varepsilon(\lambda, x) \equiv -T_0^0(\lambda, x) < -\Lambda \qquad (3.24)$$

Notice that the right hand side is parametrically large in the $G_N \to 0$ limit. Indeed, in this limit the negative curvature is fully supported by the cosmological constant term, so a flow based on geodesic foliations would be allowed for arbitrary matter content. On the other hand, if one takes $G_N$ to be small but finite, equation (3.24) from [40] would indeed provide a sharp upper bound for the energy density. Once this bound is violated, geodesics start to focus and the transverse area start to decrease instead of increase.

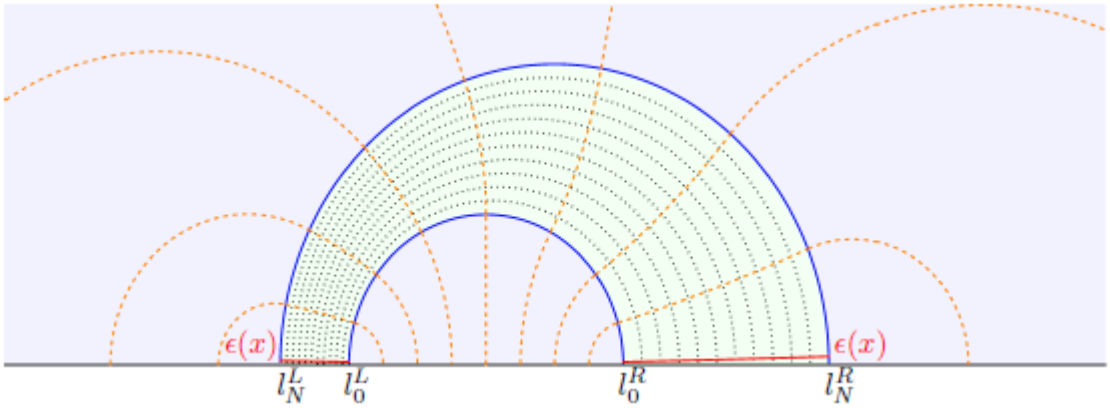


Figure 6 from [40]. A second example of a maximally packed flow. In this example, we have considered a family of intervals $A_N$ with variable left and right boundaries. The two limiting minimal surfaces $m(A_0)$ and $m(A_N)$ bound the portion of the bulk that is shaded in green. In this region, the vector $V$ has maximal norm, i.e., $|V| = 1$ and is orthogonal to the intermediate minimal surfaces $m(A_n)$. The UV cutoff that leaves the flux across the different surfaces constant is shown in red, but other choices are also allowed. The regions inside of $m(A_0)$ and outside of $m(A_N)$, which are shaded in blue, are continued with the geodesic flows constructed with the algorithm of section 2 of [40], see figure 2..

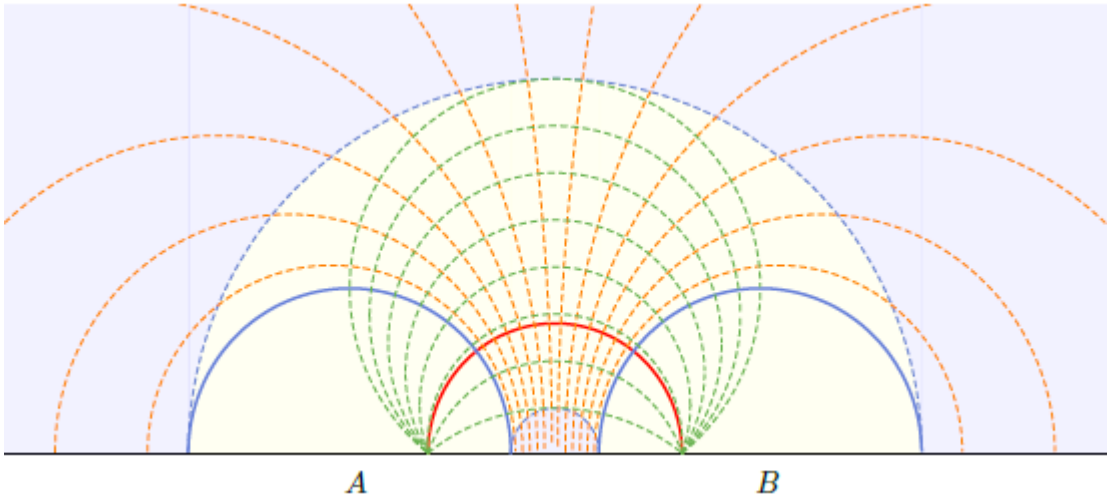


Figure 9 from [40]. A graphic illustration of the construction of a maximally packed flow for two disjoint intervals in AdS. The two intervals are of equal size and are close enough so that the entanglement wedge r(AB) (shaded in yellow) is connected. The auxiliary minimal surface $m(\tilde{A})$ is shown in red, and is picked such that it intersects orthogonally both m(A) and m(B), represented in blue. The set integral curves of the auxiliary vector field $\tilde{V}$ are shown as orange dashed lines. These integral curves interpolate smoothly between m(A) (m(B)) and $\Xi_{AB}$ so they provide a natural family of nested intervals. The level set surfaces of $\tilde{V}$ are represented by green dashed lines. They correspond to the integral curves of the maximally packed flow V that computes entanglement of purification $\varepsilon(A:B)$.

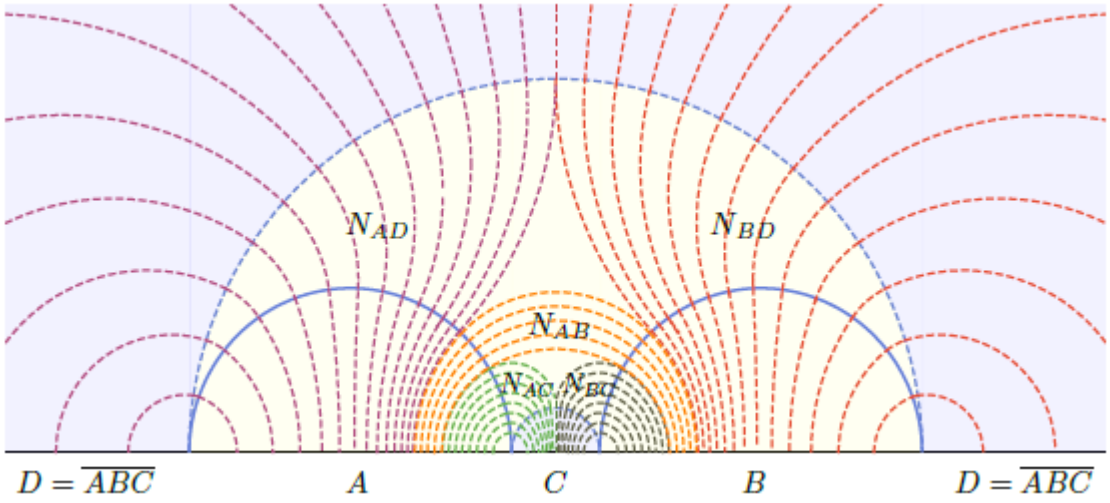


Figure 11 from [40]. In this figure we represent in different colors the individual thread bundles of the max multiflow configuration connecting the various regions in in a system of two disjoint intervals. The threads connecting the regions A and B are labeled as $N_{AB}$, A and C as $N_{AC}$, A and D as $N_{AD}$, B and C as $N_{BC}$, and B and D as $N_{BD}$. The threads

that connect A and B have the physical meaning of representing half the mutual information between A and B, I(A : B).

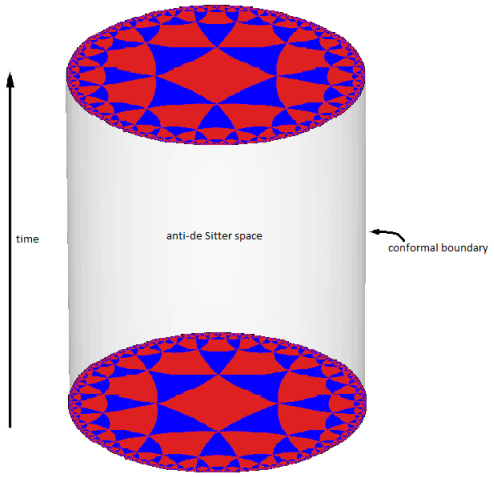


Three-dimensional anti-de Sitter space is like a stack of hyperbolic disks, each one representing the state of the universe at a given time. The resulting spacetime looks like a solid cylinder.

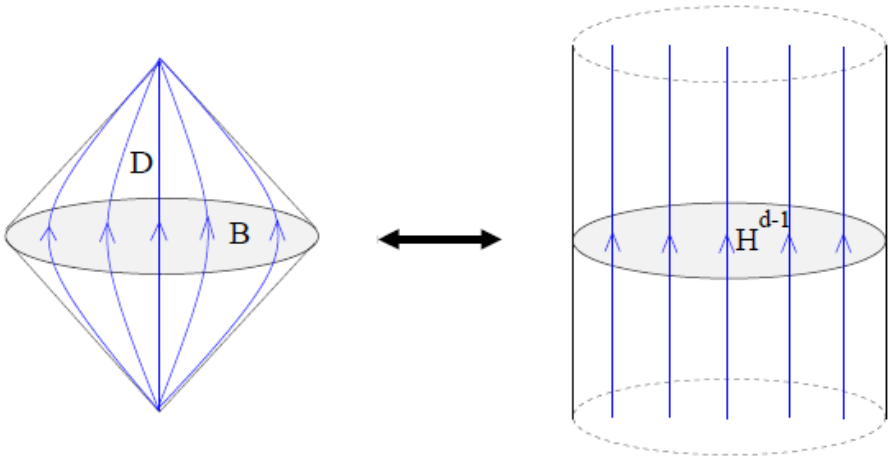


Figure 1 from [4]. Causal development D (left) of a ball-shaped region B on a spatial slice of Minkowski space, showing the evolution generated by $H_B$. A conformal transformation maps D to a hyperbolic cylinder $H^{d-1} \times time(right)$, taking $H_B$ to the ordinary Hamiltonian for the CFT on $H^{d-1}$.

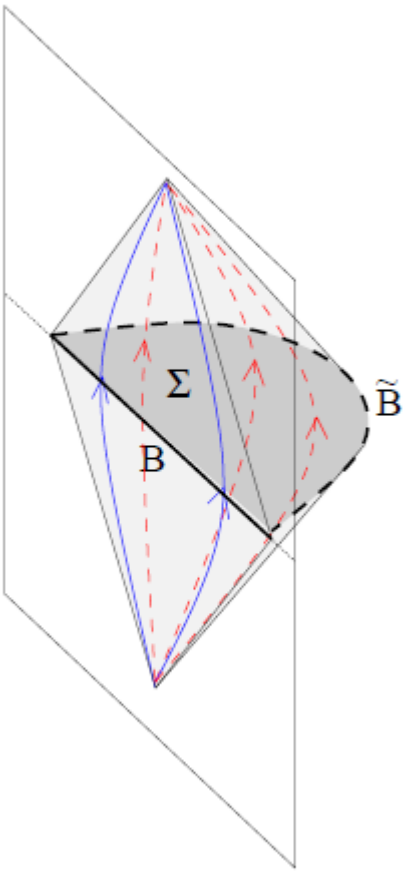


Figure 2 from [4]. AdS-Rindler patch associated with a ball $B(R, x_0)$ on a spatial slice of the boundary. Solid blue paths indicate the boundary flow associated with $H_B$ and the conformal Killing vector ζ. Dashed red paths indicate the action of the Killing vector ξ.

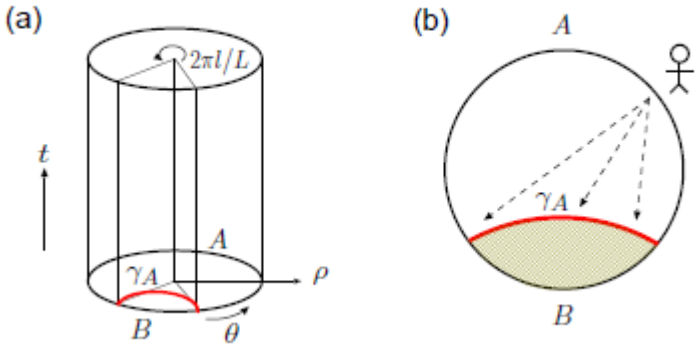


Figure 4 from [9]: (a) AdS3 space and CFT2 living on its boundary and (b) a geodesics $\gamma_A$ as a holographic screen.

Since the quarks inside BHs, as commoving particles following the collisions of the Electroweak (EW) bubbles filled with Higgs field, generate an electromagnetic field

(EM) by a pulsating process [12] with frequency $\nu = \omega^{-1}$, a such pulse of stress-energy it could be $8\pi T_{\mu\nu} k^{\mu} k^{\nu} = a\delta(\lambda)$, $a$ is a positive constant, and the surface gravity

$\kappa = \frac{c^3}{GM}[s^{-1}]$.

We can observe that $\frac{\Delta A}{A} = \frac{8\pi GM}{c^2} \cdot \frac{1}{R} = \frac{r_{Schw}}{R}$, or, we have obtained the classical formula for deformation.

### *3. Magnetic field generation in first order phase transition bubble collisions*

When the Universe supercooled below the critical temperature ($T_c \approx 100\,GeV$) the Higgs field locally tunneled from the unbroken $SU(2) \times U(1)_Y$ phase to the broken $U(1)_{em}$ phase [5].

The tunneling gave rise to the formation of broken phase bubbles which then expanded by converting the false vacuum energy into kinetic energy.

The typical size of a bubble after the phase transition is completed is in the range

$$R_{bubble} \sim f_b H_{EW}^{-1} \qquad (9)$$

Where

$$H_{EW}^{-1} \sim \frac{m_{Pl}}{g_*^{1/2} T_c^2} \approx 10\,cm \qquad (10)$$

is the size of the event horizon at the electroweak scale, $m_{Pl}$ is the Planck mass, $g_* \sim 10^2$ is the number of massless degrees of freedom in the matter, and the fractional size $f_b$ is $\sim 10^{-2} \div 10^{-3}$.

Törnkvist in [5], discusses the suggestion made in cited Ref. [9], that magnetic fields may be generated in the decay of Z -strings. It is well-known that the unstable Z -string decays initially through charged W -boson fields. The idea is that these W fields form a "condensate" which then in turn would act as a source of magnetic fields. The conventional gauge-invariant definition of the electromagnetic field tensor in the SU(2) × U(1) Yang-Mills-Higgs system is given in [9], where a possible generalization of the definition for the Weinberg-Salam model was given by Vachaspati [5]. It is conceivable, however, that the large conductivity of the plasma in the early universe, cited refs. [2, 1, 33] may cause the magnetic field lines to freeze into the fluid so that it remains preserved at later times.

To note also, that, in case of electroweak and QGP epochs the magnetogenesis is analyzed for different mechanisms [15÷18]

We can now wonder what is the strength of the magnetic fields at the end of the EWPT. A partial answer to this question has been recently given in [19] where the formation of ring-like magnetic fields in collisions of bubbles of broken phase in an abelian Higgs model were inspected.

Under the assumption that magnetic fields are generated by a process that resembles the Kibble and Vilenkin [24] mechanism, when $W$ condensate- and $Z$ strings-configurations are expected to form, it was concluded that a magnetic field is of the order

$B = 2 \times 10^{20} G \cong 2 \times 10^{16} [T]$.

Assuming turbulent enhancement of the field by inverse cascade, a root-mean-square value of the magnetic field $B_{rms} = 10^{-21} G \cong 10^{-17} [T]$ on a commoving scale of $10 Mpc \cong 3 \times 10^{23} [m]$ as from [11].

In the case of a first order electroweak phase transition, the Higgs field inside a given bubble has an arbitrary phase [19]. The bubbles expand and eventually collide, while new bubbles are continuously formed, until the phase transition is completed. This also involves the equilibration of the phases of the complex Higgs fields, the gradients of which act as a source for gauge fields, thus making the generations of magnetic fields possible. The magnetic field generated in bubble collisions will be imprinted on the background plasma.

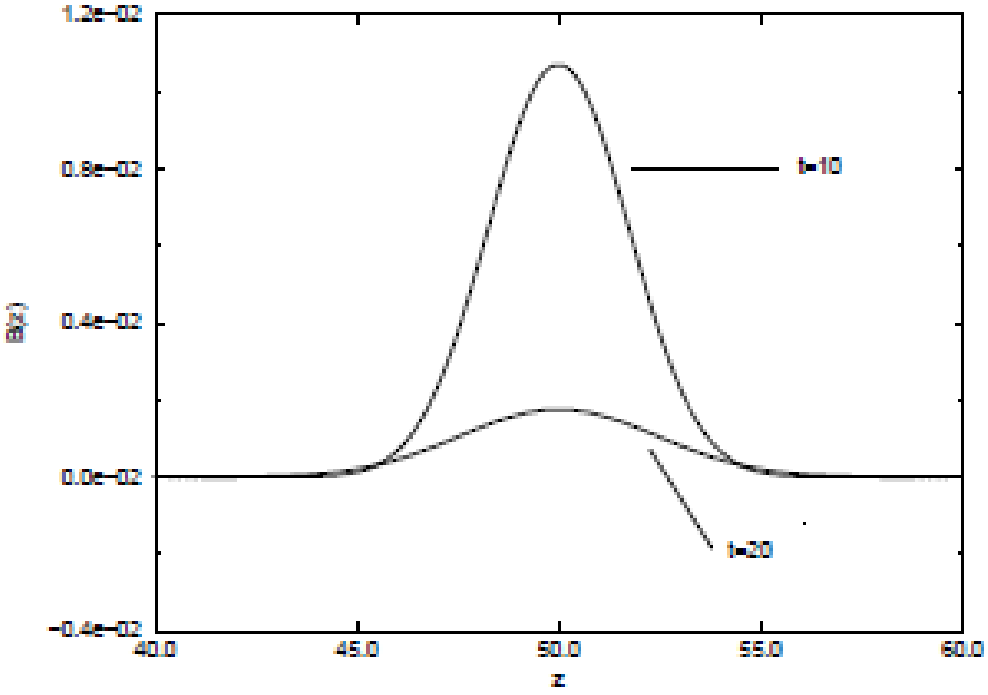

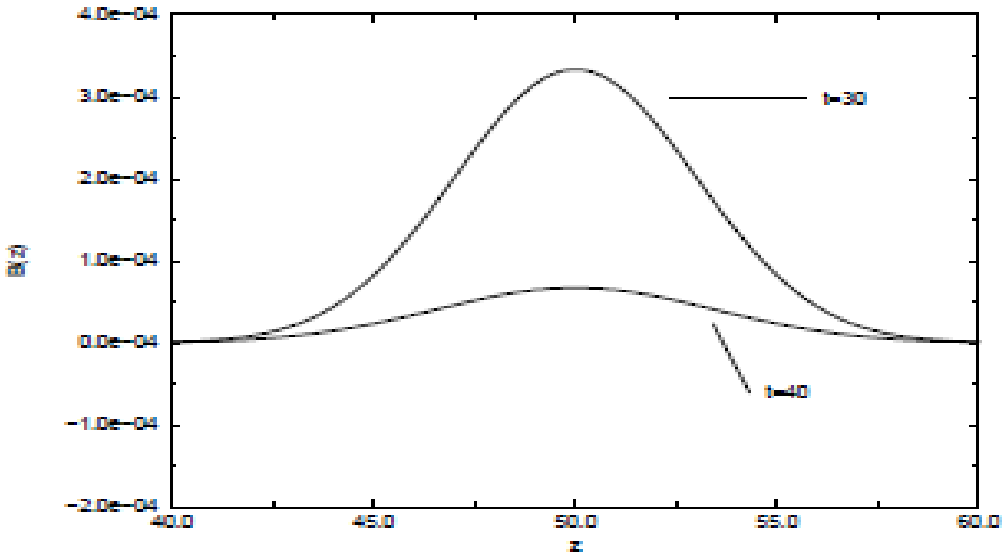


Figure 5 from [19]: B with v = 1, r = 1, σ = 7, R = 10 and t = 10, 20, 30 and 40 after the initial collision. The point of initial collision on the z-axis is $z_1 = 50$ (and units are $e\eta = 1$; the gauge boson mass $m_A = "e\eta" = T_c$ ).

It is convenient to write the Higgs field in polar form:

$\Phi = \frac{1}{\sqrt{2}} Xe^{i\theta}$ ; X settles rapidly to its equilibrium value η.

Again the magnetic field escapes from the bubbles intersection region and moves outwards with the speed of light.

**4. The born of pairs as a permanent process**

Now, the rate per unit volume of pairs creation is given by using the Schwinger effect $R$

$$R = (E/E_{cr})^2 (c/\lambda^4)(8\pi^3)^{-1} * \exp(-\pi E_{cr}/E) \quad (11)$$

or $E/E_{cr} << 1$, mass $m$ of quarks, and so-called "critical" electric field $E_{cr} = m^2 c^3 / e\eta$ ; $E$ the electric field of quarks tubes,

the volume is given by:

$V_{matter} = (\lambda_C)^4 \frac{1}{c}[m^3 s]$ ; $m$ -the mass of pairs $(W^{\pm}, q^{\pm})$.

***5. The strain at Event Horizon***

From [12] we have:

$\lambda = \kappa^{-1} e^{kv}$ ; $\kappa^{-1} = 4M$ ; $v = t + r^*$ ; $C = 1 - 2M/r$ ; and $r^* = \int C^{-1} dr$ ; $C_{,r} = 2M/r^2$

We will assume that $T_{vv}(v)$ represents ingoing radiation which changes the black hole's mass by only a small fractional amount, $|\Delta M| << M$. We can then take κ to be constant to lowest order. If we change the independent variable from λ to v = t + r*, then

$$\frac{d}{d\lambda} = e^{-\kappa v}\frac{d}{dv};\ v = 1/\omega;\kappa = \frac{c^3}{4GM}$$

And

$$T_{\mu\nu}k^{\mu}k^{\nu} = e^{-2\kappa v}T_{vv}$$

For spherically symmetric pulses, the shear and vorticity vanish, and the Raychaudhuri equation, Eq. (36) from [12], becomes

$$\frac{d\theta}{dv} = -\frac{1}{2}e^{\kappa v}\theta^2 - 8\pi e^{-\kappa v}T_{vv}(v)$$

The equation for the horizon area can be expressed as

$$\frac{dA}{dv} = e^{\kappa v}A\theta$$

If we take $A_0 = 16M_0^2$ to be the initial area of the black hole in the distant past, where $M_0$ is its initial mass, then we have

$$\frac{\Delta A}{A_0} \cong \frac{a}{\kappa}e^{\kappa v_+} = 2\frac{\Delta M}{M_0}$$

In this approximation, the change in the mass of the black hole is

$$\Delta M = \frac{a}{2\kappa}M_0 e^{\kappa v_+} = \frac{aA_0}{8\pi}e^{\kappa v}$$

where we have used $\kappa = 1/(4M) \cong 1/(4M_0)$.

This agrees with the result obtained by calculating the change in mass directly from Eq. (12) as $\dot{M} = \frac{dM}{dt} = F = \int T_t^r r^2 d\Omega$

Here, it was defined an "effective magnetic field", $B_{eff}$, in terms of the total energy density in the magnetic field of MF Vortex,

$$\varepsilon_0 = \frac{\varepsilon_0 c^2 B_{eff}^2}{8\pi} \qquad (12)$$

On the horizon, $T_t^r = T_{vv}$, $r = 2M + \varepsilon$

Since the quarks generated inside nucleons or in EW bubbles are generated by a pulsating process with frequency $v = \omega^{-1}$, a such pulse of stress-energy it could be $8\pi T_{\mu\nu}k^{\mu}k^{\nu} = a\delta(\lambda)$, $a$ is a positive constant, and the surface gravity $\kappa = \frac{c^3}{GM}[s^{-1}]$.

We can observe that $\frac{\Delta A}{A} = \frac{8\pi GM}{c^2}\cdot\frac{1}{R} = \frac{r_{Schw}}{R}$, or, we have obtained the classical formula for deformation.

**6. The Pre-formation of BH at EWPT Universe Epoch**

**First step-at EWPT epoch**

$\varepsilon_{EWPT} = 100\,GeV \to 1.7\times10^{-8}\,J$ ; $a_{end-EW} = 0.9$ ; $k_{end}^{-1} = 0.1[m]$, with eq. (6), (7) results $R = 0.4m$ and eq.(8) for $\rho = 4\times10^{28}[kg/m^3]$, or $H_{end}^{-1} = 0.1 \cong H_{EW}^{-1}[m]$,

$t_{end} = H_{end}^{-1}/c = 3.3\times10^{-10}\,s$, $n_{bit\_threads} = \dfrac{M_U c^2}{1.7\times10^{-8}} = 1.1\times10^{64}$; $k_{end}^{-1} = 0.1$;

$B_{EWPT} = 7.7\times10^{18}[T]$; $\lambda_C = 1.7\times10^{-18}$; $H_{leave}^{-1} = k_{leave}^{-1} = 10^{-18}[m]$ we found $N = 39.22$

**At BH spacetime**

From [1], the mass of M87 is appreciated as $M_U = 10^9 \times M_{SUN} = 1.98\times10^{39}\,Kg$,

, and with $\varepsilon_{BH} = 100/a_{end\_BH} = 7\times10^{-3}\,GeV = 1.12\times10^{-12}\,J$ , when, the initially $m_A \cong 100\,GeV$ at 0.1 m, at commoving distance of BH diameter this becomes $m_A = 7MeV \to B_{magnetic\_flux=} = 3.26\times10^{10}[T]$, from eq. (5), that corresponds with quarks mass.

As a rule, the build of spacetime is obtained by using well-known Inflation models as in A.H.Guth [13], $k_{end} = H_{leave}^{-1}e^N[m^{-1}]$; $a_{end} = k_{end}^{-1}/H^{-1}$ ; $H_{leave} = 0.1[m]$; $N(\varphi)$-e- folds, thus the horizon-entry is when $k_{end} = k_{leave}e^{-N}$ ; $k_{end}^{-1} = 3.5\times10^7[m]$, $a_{end\_BH} = 1.43\times10^4$, and with eq. (6), the spacetime deformation becomes $H_{end}^{-1} = R = 1.1\times10^{10}[m]$, and respectively, from eq. (7) with $\rho = 4.6\times10^7[kg/m^3]$ from eq. (8), also $H_{end}^{-1} = 5.5\times10^9[m]$; when the number of bit-threads as above is $n = n_{hologram} = 1.1\times10^{64}$; $t_{end} = H_{end}^{-1}/c \cong R/c = 1670[s]$, $T = 8.3\times10^{10}[K]$, with $H_{leave}^{-1} = k_{laeve}^{-1} = 0.1[m]$ we found $N = 19.675$ to match the iterations cycle:

$m_g \to \eta\nu \to k_B T \to \varepsilon \to R \to H_{end}^{-1} \to a_{end} \to N$.

$\lambda_{C\_BH} = 2.67\times10^{-14}[m]$, the curvature radius $R$ is equally with Schwarzschild radius $r_{sch} = 2.9\times10^{12}[m]$

**at BH diameter**

, and with $\varepsilon_{near} = 0.01/a_{end\_near} = 7\times10^{-3}\,GeV = 1.12\times10^{-12}\,J$ , at commoving distance of BH diameter $m_A = 7MeV \to B_{magnetic\_flux=} = 3.25\times10^{10}[T]$ , with eq. (5), the horizon-entry is when $k_{end} = k_{leave}e^{-N}$ ; $k_{end}^{-1} = 5\times10^{11}[m]$, $a_{end\_near} = 1$, and with eq. (6), $H_{end}^{-1} = 1.1\times10^8[m]$, and respectively near the same with eq. (7) for $\rho = 6.6\times10^{11}[kg/m^3]$ from eq. (8), and the number of bit threads is $n = n_{hologram} = 1.1\times10^{68}$; $r_{object} \approx r_{Sch}$, $t_{end} = H_{end}^{-1}/c \cong R/c = 1673[s]$, where with $H_{leave}^{-1} = k_{laeve}^{-1} = 5\times10^{11}[m]$ we found $N = 1.61$ to match the iterations cycle:

$m_g \to \eta\nu \to k_B T \to \varepsilon \to R \to H_{end}^{-1} \to a_{end} \to N$.

$\lambda_{C\_near} = 2.67\times10^{-14}[m]$

**at EHT-today**

Therefore, the new horizon of EWPT bubbles collisions, where the stress-energy pulse leaves under the form of bit threads, see figure 1., $a_{leave} = k_{leave}/H_{leave} = 1$, or $k_{leave}^{-1} = H_{leave}^{-1} = r_{Schw}$.

Now, the new horizon-entry-EHT detector is when the wave length $k_{end} = k_{leave}e^{-N}$; $k_{end}^{-1} = 8.1\times10^{14}[m]$; and the scale factor arrives at $a_{end} = k_{end}/H_{end}$ , $\varepsilon_{space} = 0.007/a_{end\_space} = 4.73\times10^{-13}GeV = 7.56\times10^{-23}J$ with Compton length $\lambda_C^{EHT\_site} = \eta/m_A c = 4\times10^{-4}[m]$; the mass being the same $M_U = 1.9\times10^{39}kg$; $a_{end\_EHT} = 1.48\times10^{10}$ and with eq. (6), the Hubble length $H_{end}^{-1} = 2\times10^{29}[m]$, the same, when the number of bit threads passing through hologram and attaining the EHT-site is $n_{bit\_threads} = \dfrac{M_U c^2}{m_A \cdot a_{end\_EHT}} = 1.06\times10^{58}$ from the total at hologram of $\cong 1.1\times10^{68}$ and , from eq. (7) with $\rho = 1.37\times10^{-29}[kg/m^3]$ from eq. (8), it results the today spacetime $H_{end\_space} = 10^{28}[m]$; and for the commoving with data for the EHT site, we have magnetic flux at $B_{magnetic\_flux=} = 1.48\times10^{-10}[T]$, with eq. (5), $t_{end} = H_{end}^{-1}/c = 4\times10^{16}s$, we found $N = 9$ to match the iterations cycle: $m_g \to \eta\nu \to k_B T \to \varepsilon \to R \to H_{end}^{-1} \to a_{end} \to N$.

In order to identify $e\eta$ in [19], and in figure 5., we proceed as following, we know that for $v = 247GeV \to \lambda_L^2 = \left(4\pi\alpha v^2/(\eta c)^2\right)^{-1} \cong 5.5e-36m^2$ , or $\lambda_L \cong 2.3e-18[m]$, which is the Compton length for $W^{\pm}$ bosons [20]. Thus, we have add one constraint equation to the four Klein-Gordon equations; the only linear, Lorentz invariant choice is

$(\Diamond + m^2)A_\mu(x) = 0$ and $\partial_\mu A^\mu = 0$ . $\Diamond = \left(\dfrac{\partial^2}{\partial t^2} - \nabla^2\right)$ is the d'Alembertian. For the time-independent case, the Klein–Gordon equation becomes

$$\left[\nabla^2 - \frac{m^2c^2}{\eta^2}\right]\psi(r) = 0 \text{; where } \frac{m^2c^2}{\eta^2} \Leftrightarrow [m^{-2}]$$

It then follows that a Klein-Gordon equation holds for A, from [19]

$$(\partial_\mu\partial^\mu + e^2\eta^2)X = 0 \text{, where } X = A_\mu$$

Introducing $\alpha^{-1} = \dfrac{4\pi\varepsilon_0\eta c}{e^2} = 137$ in $\lambda_L$ is obtained $\lambda_L^2 = "e^2\eta^2" = \left(\dfrac{e^2v^2}{\varepsilon_0(\eta c)^3}\right)^{-1}$

Therefore, in figure .7 results at the hologram site $"e\eta" = 780[m^{-1}]$; so $50/780 = 0.063[m]$ when $v = m_A/a_{end\_EHT} = 7.56\times10^{-23}[J]$, the same value is obtained

if we consider that at EHT site from the number of bit threads of initially value of $10^{68}$ it pass only $\cong 10^{58}$, in the above formula, we have for the today

$v = m_{Anear} \cdot \frac{1.06 \times 10^{58}}{1.57 \times 10^{68}} = 7.56 \times 10^{-23}[J]$, where $m_{Anear} = 1.12 \times 10^{-12}[J]$ as above, also, we have for the pulse dimension as from figure 5., $\cong 50 * 780 = 3.92 \times 10^{4}[m^{-1}]$, so the frequency is $\omega = c \cdot "e\eta" = c * 780 = 233 GHz$, which is in the range of the frequency measured in [1], *this being the decisive result which validates the present model*.

The power of a quark synchrotron emissions due of quarks moving on boundary in the magnetic field $(B)$ due of bubbles collisions, within boundary is

$P = \frac{e^2}{2\pi\varepsilon_0 c^3} a^2 n \Gamma V \Delta t = 2.2 \times 10^{-25} \xrightarrow{\times 10^{58}} 2.2 \times 10^{33}[w]$; from eq. (11) the rate of $q^+ q^-$ pairs is $\Gamma = R = 8 \times 10^{54}[m^3 s]^1; V = \lambda_C^3$, $\lambda_C = 2 \times 10^{-14}[m]$,

$\varepsilon = P\Delta t = 1.1 \times 10^{36}[J] \approx 10^{36}\, atEHT$

$a = c^2 \times 0.7^2 \frac{1}{R} = 4 \times 10^5 [m/s^2]$; $n = \frac{M_U c^2}{\varepsilon_A a_{end\_EHT}} = 1.5 \times 10^{58}$ quarks on boundary;

$\Delta t = R/0.7c = 479[s]$, $R = H_{end} = 10^{11}[m]$; if $n = 10^{58}$ as quarks at near CFT , see above, it results $\varepsilon = 10^{36}[J]$, *also, a decisive results which validate our model*. But we can also estimate the emission energy with $\varepsilon = 10^{58} * 10^{-23} = 10^{35}[J]$

**7.The hologram and the spacetime deformations**

*Near BH*

We use the above model confirmed in others author works [15÷18].

With $a = \frac{c}{R}[s^{-1}]$ ; where $R = 5 \times 10^{11}[m]$; $a = 5.9 \times 10^{-4}$ ; with $M = 10^9 \times 1.98 \times 10^{24} = 1.98 \times 10^{39}[kg]$; $\kappa = 5 \times 10^{-5}[s^{-1}]$; if we have the generation inside the vacuum of BH as given by eq. (11) , $v = \omega^{-1} = (R/V \cdot V_{vol})^{-1}$; where $R/V \times V_{vol} \cong 8.4 \times 10^{54} \cdot \lambda_C^3 = 1.61 \times 10^{14}[s^{-1}]$, $\lambda_c = \eta/mc = 2.67 \times 10^{-14}[m]$; where, the mass of ring's particles (electrons) being $m = 1.25 \times 10^{-29}[kg]$, that resulting $v = 6.2 \times 10^{-15}[s]$; and $e^{\kappa v} \cong 1.0$. Here for $E$ we uses eq. (5) , $E = 8.1 \times 10^{19}[N/C]$, with $V = 1.12 \times 10^{-12}[J]$ that corresponds to quarks mass, and the magnetic flux is $B = E/c = 3.25 \times 10^{10}[T]$. Inside the BH this flux is expelled under the form of jets with the frequency ~233 GHz.

So, the deformation near BH is $\frac{\Delta A}{A} = 11$; or $\Delta A = 5.48 \times 10^9 [m]$, just the BH's core size, or where the lensing is total (the radiation don't escapes), see figure 1.

To note that at EWPT epoch the deformation is $\frac{\Delta A}{A} = 5.8 \times 10^{13}$; or $\Delta A = 10^{13}[m]$ as the spacetime region deformation.

*At spacetime-today*

With $a = \frac{c}{R}[s^{-1}]$ ; where $R = 10^{25}[m]$; $a = 2.4 \times 10^{-17}$ ; with $M = 10^{9} \times 1.98 \times 10^{24} = 1.98 \times 10^{39}[kg]$; $\kappa = 5 \times 10^{-5}[s^{-1}]$; if we have the generation inside the BH as given by eq. (11) , $v = \omega^{-1} = (R/V \cdot V_{vol})^{-1}$; where $R/V \times V_{vol} \cong 1.7 \times 10^{14} \cdot \lambda_C^3 = 10^{4}[s^{-1}]$, $\lambda_c = \eta/mc = 4 \times 10^{-4}[m]$; where, the mass of ring's particles (electrons) being $m = 8.4 \times 10^{-40}[kg] \rightarrow 7.53 \times 10^{-23}[J]$, that resulting $v = 9.2 \times 10^{-5}[s]$; and $e^{\kappa v} \cong 1.0$. Here for $E$ we uses eq. (5) , $E = 0.37[N/C]$, with $V = 7.56 \times 10^{-23}[J]$ that corresponds to the quarks mass, and the magnetic flux is $B = E/c = 1.48 \times 10^{-10}[T]$.

So, the deformation near BH is $\frac{\Delta A}{A} = 4.9 \times 10^{-13}$; or $\Delta A = 5 \times 10^{15}[m]$, or the spacetime deformation is above the ring diameter.

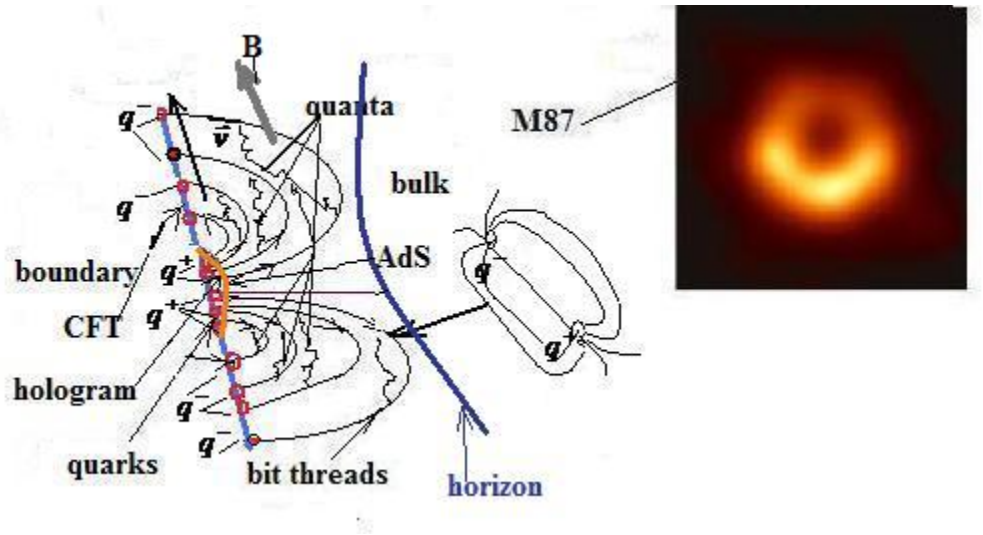


Figure 1. Our model of M87*

**8. Conclusions**

By using authors developed models, we found that

-M87 it was pre-formed when the spacetime was of 0.1 [m] or at EWPT epoch of Universe as a object of mass $\cong 10^{9} \times M_{SUN}$.

-The pulsed EM field it was generated by EWPT bubbles collisions, and at commoving distance of $10^{11} \div 10^{13}$[m] decays to quarks mass.

-The Einstein- stress energy tensor gives the spacetime deformation (H).

-This field is entangled from inside the BH region to the boundary as a hologram, where each particle (quarks-string end) is a point.

- The flow $v$ by its field lines (also called *flux lines*) with the condition $\nabla \cdot v = 0$ means that the threads cannot begin, end, split, or join in the bulk; each thread can begin and end only on a boundary, which could be the conformal boundary where the field theory lives,

or possibly a horizon (e.g. if are considering a single-sided black hole spacetime). This field lines seems with open strings with quarks ends on the boundary (CFT). In case of structured cosmic bodies (planets, stars, etc.) the quarks string forms thin tubes due of gluonic confinement, so there is not emission.
-The hologram is the place of lensing, inside its there is not emission, that gives the shadow (black hole). The field lines passing the hologram give the luminosity with the frequency of 233 GHz as it was calculated, and as being observed by EHT with some bulbs, see figure 1 (left and right).
-The gravimetric field deforms the spacetime, initially in pre-formation arriving at $r = 10^{13}[m]$ which it remains near constantly till today, - quarks pairs by Schwinger effect produce $e^{+}e^{-}$ which moving on CFT that giving the synchrotron radiation of energy $\cong 10^{36}[J] \approx 10^{36}[J]\_atEHT$ .
-The rotating body BH (as every cosmic object) being into equilibrium with his ring (the centripetal force equals the gravitational force), the attraction being extend to the deformed spacetime $r = 10^{13}[m]$.
-The EHT imagine seems to copy to figure 6, respectively of packed flow with two blobs.
-In case of others bodies: stars, planets, BHs from collapsed stars, as being constituted of mainly of nucleons, since there is a strong coupling (confining) between the quarks in nucleons and a low rotation speed, do not appear radiation emission that explain the theirs opacity, by comparison.
Therefore, again is remarkable the proof of the author models also for this cosmic object.

**References**


1. The Event Horizon Telescope Collaboration, First M87 Event Horizon Telescope Results. I. The Shadow of the Supermassive Black Hole, The Astrophysical Journal Letters, 875:L1 (17pp), 2019 April 10
2. Shawn X. Cui, et al., Bit Threads and Holographic Monogamy, arxiv:1808.05234v1 [hep-th], 2018.
3. M. Freedman and M. Headrick, Bit threads and holographic entanglement, Commun. Math. Phys. 352, 407 (2017), arXiv:1604.00354v3 [hep-th], 2017.
4. T. Faulkner, M. Guica, T. Hartman, R. C. Myers, M. Van Raamsdonk, Gravitation from entanglement in holographic CFTs, arXiv:1312.7856v2 [hep-th], 2017, J. High Energy Phys. 03 (2014) 051.
5. Ola Törnkvist, GINZBURG-LANDAU THEORY OF THE ELECTROWEAK PHASE TRANSITION AND ANALYTICAL RESULTS, arxiv:hep-ph/920.4235v1, 1992.; T. Vachaspati, Phys. Lett. B265 (1991) 258.
6. Xian-Hui Ge, Can-Can Wang, Emergence of cosmological Friedmann equations from quantum entanglement, arxiv:1709.03290v1 [gr-qc], 2017.
7. P. Calabrese and J. Cardy, "Entanglement entropy and quantum field theory: A non-technical introduction," [arXiv:quant-ph/0505193].
8. P. Calabrese and J. Cardy, "Entanglement entropy and quantum field theory," J.Stat. Mech. 0406, P002 (2004) [arXiv:hep-th/0405152]; Entanglement Entropy and Quantum Field Theory, arXiv:hep-th/0405152v3 2 Oct 2008

9. Shinsei Ryu, Tadashi Takayanagi, Holographic Derivation of Entanglement Entropy from AdS/CFT, arxiv:hep-ph/0603001v2, 2006; arXiv:hep-th/0605073v3, 2006.
10. Dario Grasso, Hector R. Rubinstein, Potentials in the Early Universe, arxiv:astro-ph/0009061v2, 2001
11. G. Vidal, J. I. Latorre, E. Rico and A. Kitaev, "Entanglement in quantum critical phenomena," Phys. Rev. Lett.90, 227902 (2003) [arXiv:quant-ph/0211074].
12. L.H. Ford, Thomas A. Roman, CLASSICAL SCALAR FIELDS AND THE GENERALIZED SECOND LAW, arXiv:gr-qc/0009076v2, 2001.
13. a) A. H. Guth and S. Y. Pi, Phys. Rev. Lett. 49 (1982) 1110; b) ALAN H. GUTH, Inflation, arxiv:astro-ph/0404546v1 27Apr 2004;
14. BICEP2 I: DETECTION OF B-mode POLARIZATION AT DEGREE ANGULAR SCALES, arxiv:1403.3985v2[astr-ph.CO] 18Mar 2014.
15. Stefan Mehedinteanu (Issue 1), On the Nature of CMBR Universe Epoch Hologram, International Journal of Advanced Research in Physical Science (IJARPS) *Volume 6, Issue 1, 2019, PP 19-30 ISSN No. (Online) 2349-7882* ***www.arcjournals.org***
16. Stefan Mehedinteanu (Issue 10), The Lensing Effect a Proof of Large Scale Entanglement in Holographic CFTs, International Journal of Advanced Research in Physical Science (IJARPS) *Volume 5, Issue 10, 2018, PP 13-23 ISSN No. (Online) 2349-7882* ***www.arcjournals.org***.
17. Stefan Mehedinteanu (Issue 11), The Entanglement in Holographic CFTs- an Alternative Explanation of the Binary Black Hole Merger (LIGO) Experiment, International Journal of Advanced Research in Physical Science (IJARPS) Volume 5, Issue 11, 2018, PP 31-42 ISSN No. (Online) 2349-7882 www.arcjournals.org.
18. Stefan Mehedinteanu, How the Entanglement Hologram Enhances the Nuclear Fusion and the Battery Effect of Light Irradiation of Hydrogen/ Deuterons Layer on Metals and Graphene, International Journal of Advanced Research in Physical Science (IJARPS) *Volume 6, Issue 3, 2019, PP 5-23 ISSN No. (Online) 2349-7882 www.arcjournals.org*
19. J. Ahonen and K. Enqvist, Magnetic field generation in first order phase transition bubble collisions, hep-ph/9704334, 1997.
20. Stefan Mehedinteanu, On the Acceleration of Beta Nuclides Decay by the Photonuclear Reaction, International Journal of Nuclear Energy Science and Engineering ( IJNESE) Volume 2, Issue 2 2012 PP. 45-56 www.ijnese.org © World Academic Publishing.
21. Tsuneo Suzuki, Katsuya Ishiguro, Yoshihiro Mori, Toru Sekido, The dual Meissner effect in SU(2) Landau gauge, arxiv:hep-lat/0410039v1, 2004.
22. L.S. Kisslinger, hep-ph/0202159
23. W.B. Kibble and A. Vilenkin, Phys. Rev. D52 (1995) 679.
24. Raphael Bousso, Holography in General Space-times, hep-th/9906022, 1999.
25. Raphael Bousso, ´Eanna ´E. Flanagan, Donald Marolf, Simple sufficient conditions for the generalized covariant entropy bound, arxiv:hep-th/0305149v1, 2003.

26. Mariano Cadoni, Maurizio Melis, Entanglement Entropy of AdS Black Holes, Entropy 2010, 12, 2244-2267; doi:10.3390/e12112244, www.mdpi.com/journal/entropy
27. Veronika E. Hubeny, Gordon W. Semenoff, Holographic Accelerated Heavy Quark-Anti-Quark Pair, arXiv:1410.1172v1 [hep-th], 2014.
28. Blandford, R. D., & Znajek, R. L. 1977, MNRAS, 179, 433.
29. K. Jensen and A. Karch, Phys. Rev. Lett. 111, 211602 (2013) [arXiv:1307.1132 [hep-th]].
30. A. Karch, A. O'Bannon, and E. Thompson, JHEP 0904, 021 (2009), arXiv:0812.3629 [hep-th].
31. Makoto Natsuume, AdS/CFT Duality User Guide, Springer, 2015 , arXiv:1409.3575v4 [hep-th], 2016.
32. Veronika E. Hubeny, Holographic dual of collimated radiation, arXiv:1012.3561v1 [hep-th], 2010
33. Yoshiki Sato, Kentaroh Yoshida, Potential Analysis in Holographic Schwinger Effect, arXiv:1304.7917v3, 2013.
34. Irene Bredberg, Cynthia Keeler, Vyacheslav Lysov, Andrew Strominger, Carg`ese Lectures on the Kerr/CFT Correspondence, arXiv:1103.2355v3 [hep-th], 2011.
35. Christiana Athanasiou ,Paul M. Chesler, Hong Liu, Dominik Nickel, Krishna Rajagopal, Synchrotron radiation in strongly coupled conformal field theories, arXiv:1001.3880v4 [hep-th], 2011.
36. Sebastian de Haro, Kostas Skenderis, Sergey N. Solodukhin, Holographic Reconstruction of Spacetime and Renormalization in the AdS/CFT Correspondence, arXiV:hep-th/0002230v3, 2000.
37. Mukund Rangamani, Tadashi Takayanagi, Holographic Entanglement Entropy, arXiv:1605.01075v1, [hep-th], 2017.
38. Ted Jacobson, Manuel Visser, Gravitational Thermodynamics of Causal Diamonds in (A)dS, arXiv:1812.01596v2 [hep-th], 2019.
39. Stefan Mehedinteanu, What would be Inside of M87* to Explain the ~~VHT~~ EHT Results, International Journal of Advanced Research in Physical Science (IJARPS), Volume 6, Issue 5, 2019, PP 20-28 ISSN No. (Online) 2349-7882 www.arcjournals.org.
40. Cesar A. Agón, Jan de Boer, Juan F. Pedraza, Geometric Aspects of Holographic Bit Threads, arXiv:1811.08879v3 [hep-th], May 2019.